Journal of Power Sources 197 (2012) 38–43

Contents lists available at SciVerse ScienceDirect

Journal of Power Sources

journal homepage: www.elsevier.com/locate/jpowsour

Electrocatalytic properties of Pd/C catalyst for formic acid electrooxidation promoted by europium oxide

Ligang Feng, Shikui Yao, Xiao Zhao, Liang Yan, Changpeng Liu, Wei Xing*

State Key Laboratory of Electroanalytical Chemistry, Changchun Institute of Applied Chemistry, Laboratory of Advanced Power Sources, Graduate School of the Chinese Academy of Sciences, 5625 Renmin Street, Changchun 130022, PR China

ARTICLE INFO

Article history:
Received 23 July 2011
Received in revised form 29 August 2011
Accepted 12 September 2011
Available online 17 September 2011

Keywords:
Direct formic acid fuel cell
Formic acid electrooxidation
Pd catalyst
Electrochemical surface area

ABSTRACT

It is found that the electrocatalytic activity and stability of Pd/C nanocatalyst for formic acid electrooxidation are enhanced by the introduction of EuOx. The morphology, composition and electrocatalytic properties of the PdEuOx/C catalyst are investigated by the transmission electronmicroscopy, energy dispersive X-ray analysis, X-ray diffraction, the linear sweep voltammetry and chronoamperometry, respectively. The EDX results confirm the existence of EuOx in the PdEuOx/C catalysts. The XRD results indicate that the Pd is in the state of face-centered cubic phase structure. The linear sweeping voltammetry and chronoamperometry measurements show that the current of formic acid electrooxidation on the PdEuOx/C catalyst is ca. 2.5 times and 9 times as high as that of the home-made Pd/C catalyst, respectively; moreover, the performances are also much higher than the commercial Pd/C catalyst. The high performances can be attributed to the larger electrochemical surface area and the electronic effect of the EuOx in the PdEuOx/C catalyst.

1. Introduction

Formic acid electrooxidation has attracted great attention due to the development of direct formic acid fuel cell (DFAFC), which is particularly suitable for portable devices with high operating power densities [1–3]. Formic acid is nontoxic, nonflammable and low crossover effect through the Nafion membrane because of the anodic repulsion between the Nafion and the partially dissociated form of formic acid [3–5]. For the formic acid electrooxidation, Pt-based and Pd-based catalysts were most frequently employed [6–11]. Generally, it was accepted that formic acid oxidation on Pt-based catalyst was mainly via an indirect path and the catalyst was easily poisoned by the adsorbed CO intermediate at low potential [12–14]. Recently, Pd-based catalysts were found to possess superior performances for formic acid oxidation in DFAFCs compared with Pt-based catalysts [7,15–18]. Moreover, due to the lower cost of Pd than Pt, considerable efforts were made to develop highly active Pd-based catalyst by alloying with other metals [19–21], optimization the catalyst preparation method [11,22–26], configuring different catalyst structure [27,28] or modifying with metal oxides [29–31]. Though the formic acid oxidation on Pd-based catalysts was mainly through the direct pathway, there was a fatal drawback of slow deactivation during the oxidation process on Pd-based catalysts. So far, the reason is not clear and the arguments are condensed on the poisoning intermediate adsorbed on the Pd surface such as the adsorption of CO, coadsorption of formate, (bi)sulfate, OH and even mass transport limitation [14,32–35]. Therefore, developing novel Pd-based electrocatalysts with highly catalytic activity and extended durability is still crucial and interesting for its practical application in DFAFCs.

The addition of metal oxides into noble metal can enhance the catalytic activity for small organic molecule electrooxidation through synergetic interaction between metal oxides and noble metals [8,29,30,36–39]. Among those, rare earth oxides exhibit a number of characteristics that make them interesting for catalytic studies due to the electronic effect. Moreover, the oxides are capable of adsorbing large quantities of OH species, which are involved in the oxidation/reduction mechanisms between the different possible oxidation states of the metal oxides. The oxygen containing species usually is beneficial to the oxidation of some poisoning intermediates. Zhou et al. reported that Eu_2O_3 in combination with Pt improved the oxidation current of the Pt/C catalyst for methanol oxidation [37]. Tian found that the rare earth ion Eu^{3+} exhibited an enhancement effect on CO and ethanol electro-oxidation in combination with the Pt electrode [40]. However, there were almost no reports of employing Eu or europium oxide (EuOx) in direct formic acid fuel cell. In order to understand the effect of europium oxide on Pd nanocatalyst for formic acid oxidation, in the present study, the PdEuOx/C catalyst was prepared and studied for formic acid oxidation. During the preparation, the hybrid EuOx/C support was firstly prepared and then the Pd was reduced onto the EuOx/C support to avoid the 'Pd hidden'; the rapid microwave

* Corresponding author. Tel.: +86 431 85262223; fax: +86 431 85685653.
E-mail address: xingwei@ciac.jl.cn (W. Xing).

0378-7753/$ – see front matter © 2011 Elsevier B.V. All rights reserved.
doi:10.1016/j.jpowsour.2011.09.030

ethylene–glycol method was used to synthesize the Pd catalyst. The structural and compositional properties of the catalysts were characterized by X-ray diffraction (XRD), energy dispersive X-ray analysis (EDX), transmission electron microscopy (TEM) and X-ray photoelectron spectroscopy (XPS). The electrocatalytic activity and durability were characterized by the linear sweeping voltammetry (LSV) and chronoamperometry (CA) for the as-prepared PdEuOx/C catalyst compared with the home-made Pd/C catalyst and the state of art commercial Pd/C catalyst for convincing. The results demonstrated that the prepared PdEuOx/C catalyst exhibited excellent catalytic activity and stability for formic acid electrooxidation.

2. Experimental

2.1. Catalyst preparation

2.1.1. EuOx/C support preparation

A proper amount of Eu_2O_3 was dissolved in 10 mL of concentrated HNO_3 and diluted in 50 mL of distilled water and ethanol (1:1 in volume ratio). Then, a given amount of Vulcan XC-72 carbon was ultrasonically dispersed into the above solution, and the solution was kept at room temperature (20 °C) under vigorous agitation for 2 h. After stirring, 0.5 M Na_2CO_3 and 1 M NaOH solution was added into the mixture to form precipitates in turn. Subsequently, the suspension was stirred overnight and finally filtered, and the solid was transferred to a tubular oven at 550 °C under the protection of nitrogen for 3 h to obtain the stable EuOx/C support.

2.1.2. PdEuOx/C catalyst preparation

Firstly, a given amount of EuOx/C hybrid support and H_2PdCl_4 solution were ultrasonically dispersed in 50 mL of ethylene glycol. And then the pH value of the suspension was adjusted by a 2 M NaOH solution to ca. 11 under ultrasonication. After that, the suspension was kept at room condition for 2 h. The suspension was then exposed in the middle of a microwave oven (LG MG-5021MW1, 2450 MHz) at 700 W with 60 s on and 15 s off for three times and cooled to room temperature naturally. Finally, the suspension was filtered, washed and dried overnight at 80 °C in a vacuum oven. The nominal content of EuOx (assuming in the form of Eu_2O_3) and Pd were 15% and 20%, respectively. All solutions were prepared using Millipore-MiliQ water and analytical-grade reagents. The home-made Pd/C catalyst was prepared by the above method and denoted as Pd/C–H. A commercial Pd/C catalyst (Aldrich Co.) denoted as Pd/C–C was also compared for the electrochemical characterization. The nominal content of Pd in all the catalysts was 20%.

2.2. Physical characterization

The X-ray diffraction (XRD) patterns were obtained using a Rigaku-D/MAX-PC 2500 X-ray diffractometer with the Cu Kα (λ = 1.5405 Å) as a radiation source operating at 40 kV and 200 mA. The composition of catalyst was determined by energy dispersive X-ray analysis (EDX) on a JEOL JAX-840 scanning electron microscope operating at 20 kV. X-ray photoelectron spectroscopy (XPS) measurements were carried out using a Kratos XSAM-800 spectrometer with an Mg Kα radiator. The transmission electron microscope (TEM) images were obtained by using a JEOL 2010 microscope operating at 200 kV.

2.3. Electrochemical measurements

The electrochemical measurements were performed with an EG&G Par potentiostat/galvanostat (Model 273A Princeton Applied Research Co. USA) and a conventional three compartment electrochemical cell. A Pt plate and Ag/AgCl electrode were used as the counter and reference electrodes, respectively. All the potentials were quoted against the reference Ag/AgCl electrode. The working electrode was prepared as follows. First, 5 mg of the catalyst was dispersed ultrasonically in 1 mL of the alcohol solution containing 50 μL Nafion solution (5 wt%, Aldrich Co., USA). Second, 10 μL of the above solution was pipetted and spread on a mirror-finished glassy carbon electrode with 3 mm diameter. At last, it was dried at room temperature for 30 min. The glassy carbon electrode was polished with alumina slurry of 0.5 and 0.03 μm successively before use. The current was normalized to the apparent surface area of the glassy carbon electrode (0.07 cm^2).

All electrochemical measurements were carried out in a 0.5 M H_2SO_4 solution with or without 0.5 M HCOOH deaerated by pure nitrogen for 15 min prior to any measurements. For the electrooxidation of formic acid, the potential range was from −0.2 to +0.8 V. The CO_{ad} stripping voltammograms were measured in a 0.5 M H_2SO_4 solution. CO was purged into the 0.5 M H_2SO_4 solution for 15 min to allow the complete adsorption of CO onto the catalyst when the working electrode was kept at 0 mV vs. Ag/AgCl electrode, and excess CO in the electrolyte was purged out with N_2 for 15 min. The amount of CO_{ad} was evaluated by integration of the CO_{ad} stripping peak. All the measurements were carried out at room temperature and the stable results were reported.

3. Results and discussion

3.1. XRD, TEM, EDX and XPS characterization

Fig. 1 shows the XRD patterns of PdEuOx/C, Pd/C–C, Pd/C–H catalysts as well as the support of EuOx/C and carbon. The peak at ca. 25° in both PdEuOx/C catalyst and EuOx/C support was evidently attributed to the (0 0 2) plane reflection of Vulcan XC-72 carbon. As it can be seen, in addition to the peak of carbon at ca. 25°, there were some other diffraction peaks in the EuOx/C support indicating the existence of EuOx. The diffraction peaks at ca. 39, 46, 68 and 82° in the PdEuOx/C, Pd/C–C and Pd/C–H catalysts corresponded to the face-centered cubic phase of Pd. However, there were no other distinct reflection peaks in the PdEuOx/C spectra which could be assigned to the EuOx. During the preparation, it was difficult to form PdEu alloy due to the mild reduction condition that was impossible to reduce the EuOx to metallic state. Because of the basic condition, the EuOx should be in the state of metal oxide or metal hydroxide

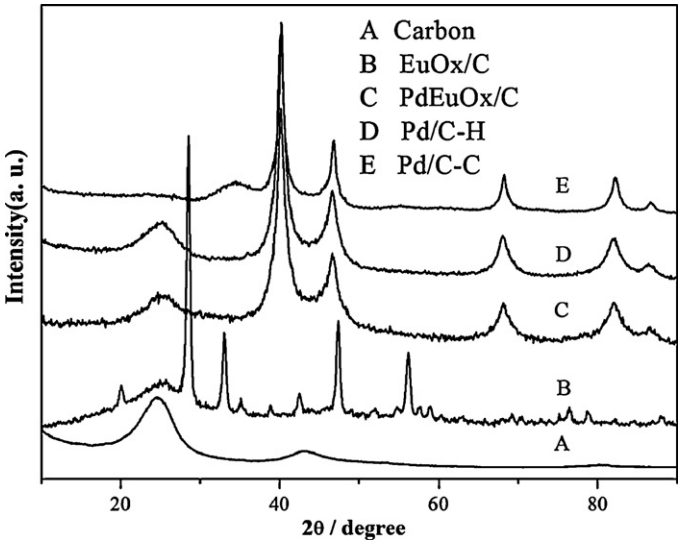

Fig. 1. XRD patterns of PdEuOx/C, Pd/C–C, Pd/C–H catalysts and the EuOx/C support and carbon.

and the EuOx may have an amorphous structure as some similar results were also observed in other reports such as $PdMoO_x$/C [30], Pt(PrCeOx)/C [39] and other Pt rare earth oxides [41]. However, the disappearance of EuOx peak on the PdEuOx/C catalyst was probably due to the low content of the EuOx because of the Pd covering up the EuOx. It can also be seen a peak at ca. 34° in the Pd/C–C catalyst which can be attributed to the reflection of Pd oxide [42]. The average crystallite sizes of the PdEuOx/C catalyst can be estimated by using the Scherrer equation after background subtraction. In the XRD pattern of Pd/C catalyst, the (2 2 0) diffraction peak at ca. 68° of Pd was far from the background signal and thus it was chosen for the calculation. The average crystallite size was about 4.0 nm, 5.4 nm and 6.8 nm for PdEuOx/C, Pd/C–H and Pd/C–C catalysts respectively.

The compositions of the PdEuOx/C catalyst were characterized by EDX and the spectrum is shown in Fig. 2. The peak of C, O, Pd and Eu can be clearly seen from the figure. The weight percentages of Pd and Eu in the PdEuOx/C catalyst were 22% and 12%, respectively. The oxygen was mainly from both the oxygen-containing groups on the Vulcan XC-72 carbon support and the oxides or hydroxides of Pd or Eu. Here, assuming that the EuOx was mainly in the form of Eu_2O_3, the weight percentage of EuOx was 14%. The above content of Pd and EuOx was consistent with the nominal results. The TEM image of the Pd/C–H catalyst is shown in Fig. 3A and the corresponding histogram of the size distribution is shown in Fig. 3B. As can be seen, most of the Pd nanoparticles were dispersed in the range of 3–7 nm on the carbon support. The average particle size of Pd revealed by the size distribution histogram was approximately 5.5 nm, which was close

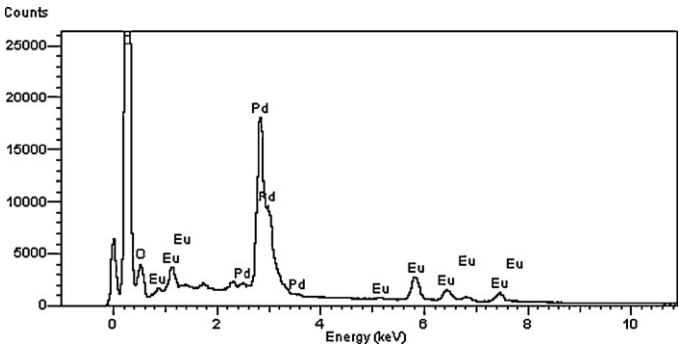

Fig. 2. EDX spectrum of PdEuOx/C catalyst.

to the XRD result. The TEM image of the PdEuOx/C catalyst is shown in Fig. 3C and the corresponding histogram of the size distribution is shown in Fig. 3D. Most of the Pd nanoparticles were uniformly dispersed on the EuOx/C support with a narrow size distribution. The average particle size of Pd revealed by the size distribution histogram was approximately 3.5 nm, which was also close to the XRD result. This result indicated that the EuOx in the carbon as anchor sites was beneficial to the dispersion of Pd nanoparticles.

XPS was used to determine the electronic property of the catalysts. Fig. 4 displays the Pd 3d spectra of the Pd/C–C, Pd/C–H and PdEuOx/C catalysts. There were two distinct peaks for the Pd $3d_{5/2}$ and Pd $3d_{3/2}$ regions in the Pd/C–C catalyst. The right small peak in

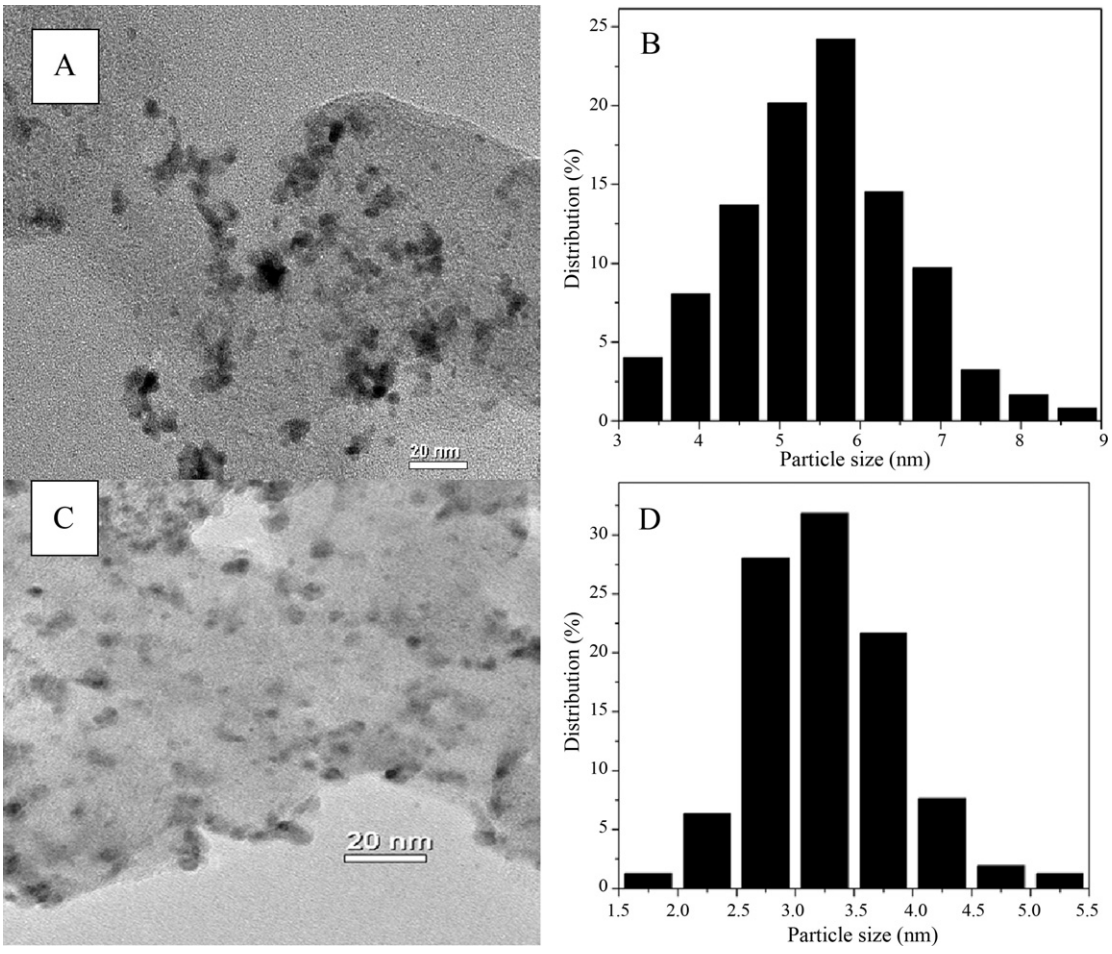

Fig. 3. TEM image of Pd/C–H catalyst (A) and the histogram of particle size distribution (B). TEM image of PdEuOx/C catalyst (C) and the histogram of particle size distribution (D).

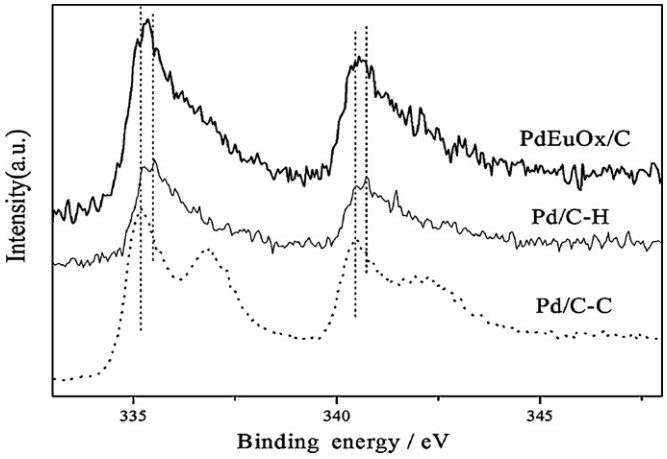

Fig. 4. XPS spectra of Pd 3d (A) for PdEuOx/C, Pd/C–C and Pd/C–H catalysts.

each Pd 3d region could be attributed to the Pd (II) species such as the Pd oxides or hydroxides. Though the peaks for the Pd (II) species were not obvious in the home-made Pd catalysts, the existent of Pd oxides cannot be ruled out because the Pd metal was easily oxidized to the form of Pd oxide (Pd^{2+}) at ambient conditions [43,44]. However, it was evident that the content of Pd oxides in the Pd/C–C catalyst was larger than that in the prepared Pd/C–H and PdEuOx/C catalysts and that was consistent with the result from XRD characterization that the peak of Pd oxide can be only seen in the Pd/C–C catalyst. Generally, it was considered that the shift of the Pd 3d position for the Pd catalysts would produce effect on the catalytic properties by so-called electronic effect. The position of C 1s for all the Pd catalysts was at about 284.6 eV; Referred to the main peak of C 1s, the positions of Pd 3d in the PdEuOx/C catalyst shifted a little to the negative direction compared with the home-made Pd/C–H catalyst. This may indicate an interaction between the Pd and the EuOx/C support, and this electronic effect can weaken the bond energy between metal and strongly adsorbed poison species which has been reported intensively [19,45]. Compared with the Pd/C–C catalyst, the positions of Pd 3d in the as-prepared PdEuOx/C and Pd/C–H catalysts were a little positive shift and it was possible due to the different catalyst preparation or composition, etc. The Eu 3d XPS spectra of PdEuOx/C catalyst and EuOx/C support are also shown in Fig. 5. The binding energy of the Eu ($3d_{5/2}$) and Eu ($3d_{3/2}$) peaks was at 1136 and 1166 eV, respectively. However, the intensity of Eu ($3d_{5/2}$) and Eu ($3d_{3/2}$) peaks was reduced largely and even disappeared on the spectrum of PdEuOx/C catalyst. This

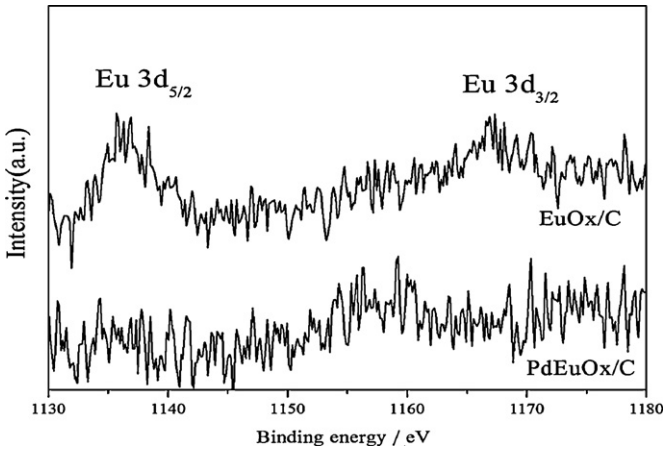

Fig. 5. XPS spectra of Eu 3d for the PdEuOx/C catalyst and EuOx/C support.

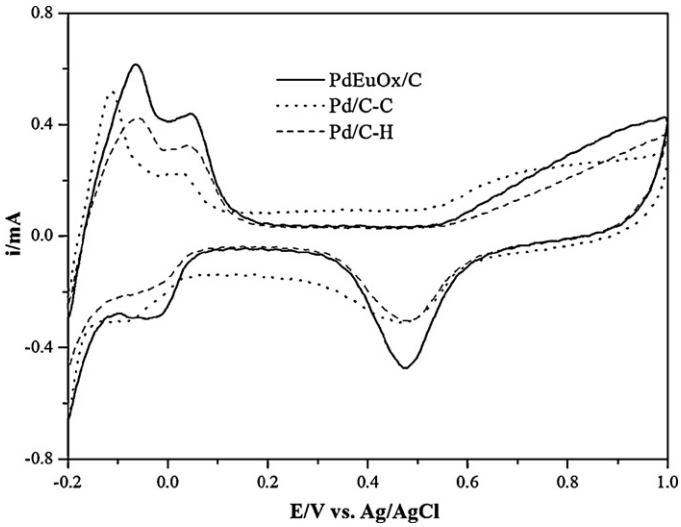

Fig. 6. Cyclic voltammograms of the PdEuOx/C, Pd/C–C and Pd/C–H catalysts in 0.5 M H_2SO_4 with a scan rate of 50 mV s^{-1}.

result was consistent with the XRD result. The Pd was mainly covering up the EuOx due to the synthetic procedure and that might be the reason for the low EuOx intensity on the XPS of PdEuOx/C and the disappearance of EuOx peaks on the XRD of PdEuOx/C.

3.2. Hydrogen and CO stripping measurements

Fig. 6 displays the CVs of the PdEuOx/C, Pd/C–C and Pd/C–H catalysts in 0.5 M H_2SO_4 solution at the scan rate of 50 mV s^{-1}. Clearly, in addition to the hydrogen adsorption and desorption peaks, the peaks for Pd oxidation and reduction were obviously observed. The position of the weak hydrogen desorption peak for the PdEuOx/C catalyst was in the middle of the peaks for Pd/C–C and Pd/C–H catalysts, while the strong hydrogen desorption peak and Pd oxide reduction peak of the PdEuOx/C Pd/C–C and Pd/C–H catalysts were much close. As the hydrogen oxidation was a surface sensitive process [46], the introduction of EuOx into the Pd/C catalyst could change the surface adsorption properties but did not change the innate properties of Pd. The hydrogen desorption peak of PdEuOx/C catalyst was largest among the three catalysts indicating a largest electrochemical surface area (ESA). Specifically, the electrochemical surface area of PdEuOx/C, Pd/C–H and Pd/C–C catalysts was 102, 85 and 73 m^2 g^{-1}, respectively. The CO_{ad} oxidation peak after subtracting the base-current is shown in Fig. 7. Clearly, the onset and the peak potentials for CO_{ad} oxidation on Pd/C–C catalyst were more negative compared with our prepared PdEuOx/C and Pd/C–H catalysts. From the XPS, there were more Pd oxides in the Pd/C–C catalyst; the oxygen containing species was beneficial to the oxidation of CO intermediate which could account for the more negative CO oxidation peak in the Pd/C–C catalyst. However, it was more reasonable to compare the PdEuOx/C and Pd/C–H catalysts prepared in the same method; the CO_{ad} oxidation peak of PdEuOx/C shifted a little negatively compared with the Pd/C–H catalyst. This result indicated that the existence of EuOx in the PdEuOx/C catalyst could promote the CO oxidation and it can be explained by the electronic effect, although it could also perhaps be explained by a bi-functional mechanism in which EuOx could provide more oxygen-containing sites for –OH formation at lower potentials than on pure Pd. Here, it should also be pointed out that the position shift for CO oxidation would not affect the formic acid oxidation largely because the CO_{ad} poisoning effect on Pd catalyst was very slow and was not severely as that on Pt catalyst [33,47]. We can also employ the CO_{ad} oxidation charge to calculate the ESA of the

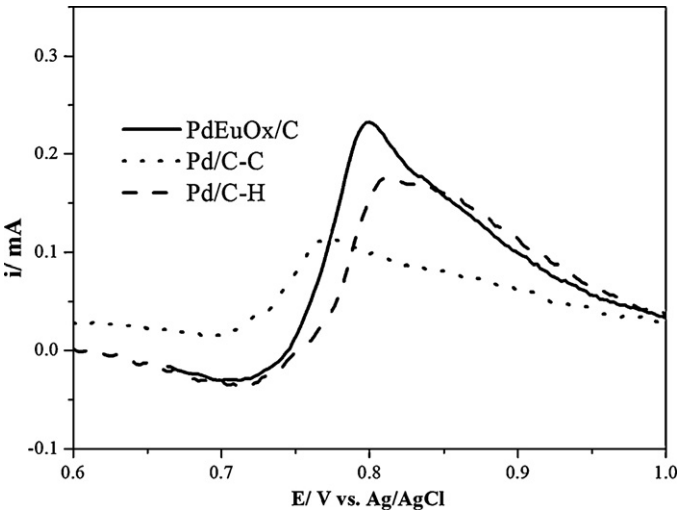

Fig. 7. CO_{ad} oxidation peak for the PdEuOx/C, Pd/C–C and Pd/C–H catalysts from the CO_{ad} stripping voltammetry.

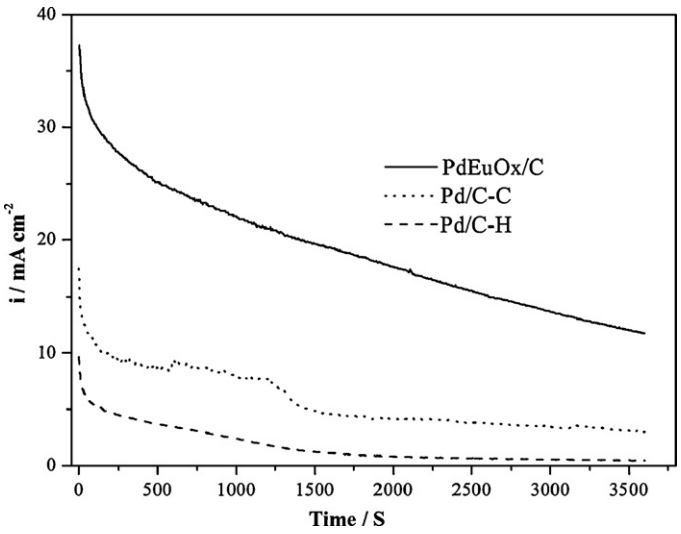

Fig. 9. Chronoamperometric curves of the PdEuOx/C, Pd/C–C and Pd/C–H catalysts in 0.5 M H_2SO_4 + 0.5 M HCOOH at 0.2 V.

catalysts. It was 70, 56 and 49.5 $m^2\,g^{-1}$ for PdEuOx/C, Pd/C–H and Pd/C–C catalysts, respectively. The results were a little smaller than those obtained from the hydrogen stripping method because of the hydrogen absorption properties of Pd; usually, the ESA obtained from that method was overestimated [48]. But these two methods were also suitable to roughly estimate the ESA of Pd catalysts.

3.3. Formic acid electroxidation

The formic acid electrooxidation on the PdEuOx/C, Pd/C–C, and Pd/C–H catalysts is shown in Fig. 8 by LSV measurements in 0.5 M H_2SO_4 and 0.5 M HCOOH at 20 mV s^{-1}. Clearly, the current of PdEuOx/C catalyst was highest among the three Pd catalysts. The peak current of PdEuOx/C catalyst was 70 mA cm^{-2} at about 0.33 V; the peak current of Pd/C–C was ca. 40 mA cm^{-2} at about 0.30 V and it was ca. 28.8 mA cm^{-2} as about 0.31 V for Pd/C–H catalyst. Compared with the Pd/C–C and Pd/C–H catalysts, the peak position of PdEuOx/C catalyst was a little positive shift. Usually, from this aspect, it was thought that the formic acid electrooxidation on the two Pd/C catalysts was much easier. However, there was a particle size effect of Pd catalysts for formic acid oxidation according to the report of Zhou and Lee [49]; namely, the peak position for formic acid electrooxidation shifted positively with the decrease of Pd particle size [49]. However, the shift of the peak position was small and that did not affect the catalytic performances largely. Moreover, the peak current of the PdEuOx/C catalyst was about two times as high as that of Pd/C–C catalyst and this could be attributed to the different catalyst preparation, composition, small particle size and so on. Compared with Pd/C–H catalyst, the peak current of PdEuOx/C catalyst was increased about 2.5 times. Here the peak current normalized to the ESA was used to compare the intrinsic activity. It was 0.74 mA cm^{-2} and 0.43 mA cm^{-2} for PdEuOx/C and Pd/C–H, respectively. The result meant that the current of PdEuOx/C catalyst was about 1.72 times that of Pd/C catalyst. By comparing the above ESA from the CO stripping method, the ESA of PdEuOx/C catalyst was about 1.42 times that of Pd/C catalyst. Therefore, this activity increase should be evidently attributed to the introduction of EuOx by the large ESA, electronic effect and so on. Here, it can also be inferred that the CO_{ad} intermediate should not affect the formic acid oxidation performances largely. As from the CO_{ad} stripping measurements, the CO_{ad} oxidation was more easily on Pd/C–C catalyst than PdEuOx/C catalyst, but the formic acid oxidation current was not larger. This result was consistent with the report of Miyake et al. that the poisoning of the Pd surface by CO, formed by dehydration of formic acid, is very slow and scarcely affects formic acid oxidation [47].

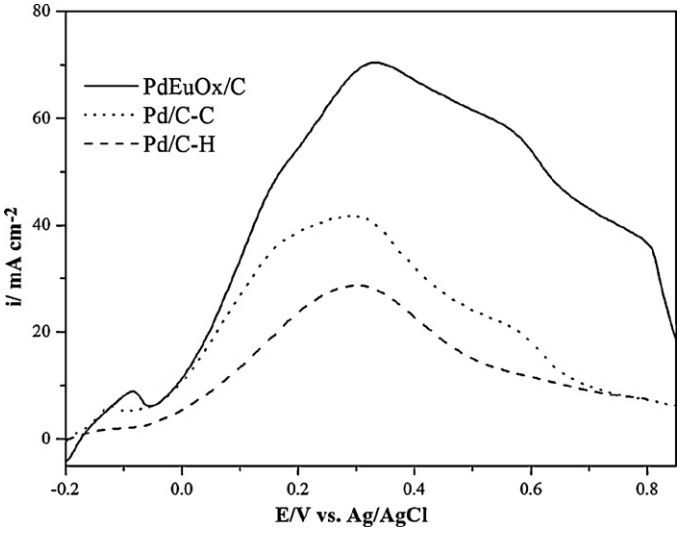

Fig. 8. Linear sweeping voltammetry of the PdEuOx/C, Pd/C–C and Pd/C–H catalysts in 0.5 M H_2SO_4 + 0.5 M HCOOH with a scan rate of 20 mV s^{-1}.

The formic acid oxidation stability of the PdEuOx/C, Pd/C–H and Pd/C–C catalysts is compared in Fig. 9 in 0.5 M H_2SO_4 and 0.5 M HCOOH at 0.2 V. The results were obtained after the above electrochemical test. It can be seen that the initial current was somewhat decreased compared to the corresponding current at 0.2 V in the above LSVs indicating a slow poisoning effect on the catalysts. From Fig. 9, the current of PdEuOx/C catalyst was largest in the whole range among the three catalysts. Specifically, the current at 1000 s on PdEuOx/C catalyst was 22 mA cm^{-2} about 3 times higher than that of 7.9 mA cm^{-2} for Pd/C–C catalyst. After 3600 s, the current on PdEuOx/C catalyst was 12 mA cm^{-2} about 4 times higher than that of 3 mA cm^{-2} for Pd/C–C catalyst. The current of Pd/C–H catalyst was lowest among the three catalysts. For example, the current at 1000 s was 2.5 mA cm^{-2} about 1/9 of the PdEuOx/C catalyst and 1/3 of the Pd/C–C catalyst; it was 0.5 mA cm^{-2} at 3600 s about 1/24 of the PdEuOx/C catalyst and 1/6 of the Pd/C–C catalyst. Therefore, it can be said that the formic acid oxidation stability on the Pd/C catalyst could be increased by the introduction of EuOx. From the above

discussion, compared with Pd/C–H catalyst, it can be verified that the introduction of EuOx/C into the Pd catalysts was very important for improving the performances of formic acid electrooxidation due to the large ESA, electronic effect or oxygen-containing species produced by EuOx; Compared with the Pd/C–C catalyst, the prepared PdEuOx/C catalyst exhibited much higher catalytic activity and stability for formic acid electrooxidation. Therefore, the novel PdEuOx/C could be used as a promising anodic catalyst for DFAFC.

4. Conclusion

The present work demonstrated that the PdEuOx/C catalyst was a promising catalyst with excellent catalytic and stability for formic acid oxidation. The EDX confirmed the existence of EuOx in the PdEuOx/C catalyst. The XRD patterns indicated that the Pd was in the state of face-centered cubic structure and the disappearance of EuOx peaks was primarily due to the Pd covering up the EuOx. The average particle size of Pd in the PdEuOx/C catalyst was about 3.5 nm within a narrow size distribution. The hydrogen and CO stripping voltammetry showed the PdEuOx/C catalyst had the largest ESA among the three Pd catalysts. The formic acid electrooxidation activity and stability of PdEuOx/C catalyst were largely improved as compared with the Pd/C–C catalyst and Pd/C–H catalyst. The significant improvements in the catalytic activity and stability could be attributed to the large ESA and the electronic effect produced by EuOx.

Acknowledgments

This work was supported by the High Technology Research Program (863 program 2007AA05Z159, 2007AA05Z143) of Science and Technology Ministry of China, and the National Natural Science Foundation of China (20933004, 21011130027, 20703043, 20876153, and 21073180) and the Science & Technology Research Programs of Jilin Province (20102204).

References

[1] C. Rice, S. Ha, R.I. Masel, P. Waszczuk, A. Wieckowski, T. Barnard, J. Power Sources 111 (2002) 83–89.
[2] P. Hong, S. Liao, J. Zeng, X. Huang, J. Power Sources 195 (2010) 7332–7337.
[3] X. Yu, P.G. Pickup, Electrochim. Acta 55 (2010) 7354–7361.
[4] J. Yeom, R.S. Jayashree, C. Rastogi, M.A. Shannon, P.J.A. Kenis, J. Power Sources 160 (2006) 1058–1064.
[5] Y.W. Rhee, S.Y. Ha, R.I. Masel, J. Power Sources 117 (2003) 35–38.
[6] E.I. Santiago, G.A. Camara, E.A. Ticianelli, Electrochim. Acta 48 (2003) 3527–3534.
[7] C. Rice, S. Ha, R.I. Masel, A. Wieckowski, J. Power Sources 115 (2003) 229–235.
[8] L. Feng, L. Yan, Z. Cui, C. Liu, W. Xing, J. Power Sources 196 (2011) 2469–2474.
[9] R. Larsen, S. Ha, J. Zakzeski, R.I. Masel, J. Power Sources 157 (2006) 78–84.
[10] G.J. Zhang, Y.E. Wang, X. Wang, Y. Chen, Y.M. Zhou, Y.W. Tang, L.D. Lu, J.C. Bao, T.H. Lu, Appl. Catal. B: Environ. 102 (2011) 614–619.
[11] Z. Bai, L. Yang, Y. Guo, Z. Zheng, C. Hu, P. Xu, Chem. Commun. 47 (2011) 1752–1754.
[12] J.D. Lovic, A.V. Tripkovic, S.L. Gojkovic, K.D. Popovic, D.V. Tripkovic, P. Olszewski, A. Kowal, J. Electroanal. Chem. 581 (2005) 294–302.
[13] V.M. Jovanovic, D. Tripkovic, A. Tripkovic, A. Kowal, J. Stoch, Electrochem. Commun. 7 (2005) 1039–1044.
[14] M. Osawa, K.-i. Komatsu, G. Samjeské, T. Uchida, T. Ikeshoji, A. Cuesta, C. Gutiérrez, Angew. Chem. Int. Ed. 50 (2011) 1159–1163.
[15] Y. Zhou, J. Liu, J. Ye, Z. Zou, J. Ye, J. Gu, T. Yu, A. Yang, Electrochim. Acta 55 (2010) 5024–5027.
[16] V. Grozovski, J. Solla-Gullón, V.C. Climent, E. Herrero, J.M. Feliu, J. Phys. Chem. C 114 (2010) 13802–13812.
[17] R. Larsen, J. Zakzeski, R.I. Masel, Electrochem. Solid-State Lett. 8 (2005) A291–A293.
[18] K. Brandt, M. Steinhausen, K. Wandelt, J. Electroanal. Chem. 616 (2008) 27–37.
[19] Z.H. Zhang, J.J. Ge, L.A. Ma, J.H. Liao, T.H. Lu, W. Xing, Fuel Cells 9 (2009) 114–120.
[20] X.W. Yu, P.G. Pickup, J. Power Sources 192 (2009) 279–284.
[21] Y. Suo, I.M. Hsing, Electrochim. Acta 56 (2011) 2174–2183.
[22] Y.J. Huang, X.C. Zhou, J.H. Liao, C.P. Liu, T.H. Lu, W. Xing, Electrochem. Commun. 10 (2008) 621–624.
[23] B.K. Jena, S.C. Sahu, B. Satpati, R.K. Sahu, D. Behera, S. Mohanty, Chem. Commun. 47 (2011) 3796–3798.
[24] H.Q. Li, G.Q. Sun, Q. Jiang, M.Y. Zhu, S.G. Sun, Q. Xin, J. Power Sources 172 (2007) 641–649.
[25] S. Zhang, Y. Shao, G. Yin, Y. Lin, J. Power Sources 195 (2010) 1103–1106.
[26] N. Cheng, R.A. Webster, M. Pan, S. Mu, L. Rassaei, S.C. Tsang, F. Marken, Electrochim. Acta 55 (2010) 6601–6610.
[27] Y.J. Huang, X.C. Zhou, J.H. Liao, C.P. Liu, T.H. Lu, W. Xing, Electrochem. Commun. 10 (2008) 1155–1157.
[28] G. Lu, A. Crown, A. Wieckowski, J. Phys. Chem. B 103 (1999) 9700–9711.
[29] X. Wang, J. Wang, Q. Zou, Y. Xia, Electrochim. Acta 56 (2011) 1646–1651.
[30] L. Feng, Z. Cui, L. Yan, W. Xing, C. Liu, Electrochim. Acta 56 (2011) 2051–2056.
[31] Q. Yi, W. Huang, X. Liu, G. Xu, Z. Zhou, A. Chen, J. Electroanal. Chem. 619-620 (2008) 197–205.
[32] H. Jeon, S. Uhm, B. Jeong, J. Lee, Phys. Chem. Chem. Phys. 13 (2011) 6192–6196.
[33] Y.X. Chen, M. Heinen, Z. Jusys, R.J. Behm, Langmuir 22 (2006) 10399–10408.
[34] R. Chenitz, J.-P. Dodelet, J. Electrochem. Soc. 157 (2010) B1658–B1664.
[35] C. Du, M. Chen, W. Wang, G. Yin, P. Shi, Electrochem. Commun. 12 (2010) 843–846.
[36] Y. Bai, J. Wu, J. Xi, J. Wang, W. Zhu, L. Chen, X. Qiu, Electrochem. Commun. 7 (2005) 1087–1090.
[37] J.H. Zhou, J.P. He, T. Wang, X. Chen, D. Sun, Electrochim. Acta 54 (2009) 3103–3108.
[38] J.W. Guo, T.S. Zhao, J. Prabhuram, R. Chen, C.W. Wong, J. Power Sources 156 (2006) 345–354.
[39] Z. Tang, G. Lu, Appl. Catal. B: Environ. 79 (2008) 1–7.
[40] T. Tian, C.P. Liu, H.H. Liao, W. Xing, T.H. Lu, J. Power Sources 174 (2007) 176–179.
[41] A.O. Neto, A.Y. Watanabe, M. Brandalise, M.M. Tusi, R.M. de, S. Rodrigues, M. Linardi, E.V. Spinacé, C.A.L.G.O. Forbicini, J. Alloy Compd. 476 (2009) 288–291.
[42] M. Ren, Y. Kang, W. He, Z. Zou, X. Xue, D.L. Akins, H. Yang, S. Feng, Appl. Catal. B: Environ. 104 (2011) 49–53.
[43] M. Ohashi, K.D. Beard, S. Ma, D.A. Blom, J. St-Pierre, J.W. Van Zee, J.R. Monnier, Electrochim. Acta 55 (2010) 7376–7384.
[44] L. Feng, F. Si, S. Yao, W. Cai, W. Xing, C. Liu, Catal. Commun. 12 (2011) 772–775.
[45] J.L. Haan, K.M. Stafford, R.I. Masel, J. Phys. Chem. C 114 (2010) 11665–11672.
[46] J.Y. Wang, Y.Y. Kang, H. Yang, W.B. Cai, J. Phys. Chem. C 113 (2009) 8366–8372.
[47] H. Miyake, T. Okada, G. Samjeske, M. Osawa, Phys. Chem. Chem. Phys. 10 (2008) 3662–3669.
[48] S.M. Senthil Kumar, J. Soler Herrero, S. Irusta, K. Scott, J. Electroanal. Chem. 647 (2010) 211–221.
[49] W. Zhou, J.Y. Lee, J. Phys. Chem. C 112 (2008) 3789–3793.